

Machine learning for acute toxicity prediction using high-throughput

enzyme-reaction chip

Qiannan Duan,^{a, b} Jianchao Lee,^{a, *} Jinhong Gao,^a Jiayuan Chen,^a Yachao Lian,^a Zoudi Wang,^c Can Wang,^d
Zhaoyi Xu,^b Juan Ren,^c Sifan Bi^a

^a Department of Environment Science, Shaanxi Normal University, Xi'an 710062, China

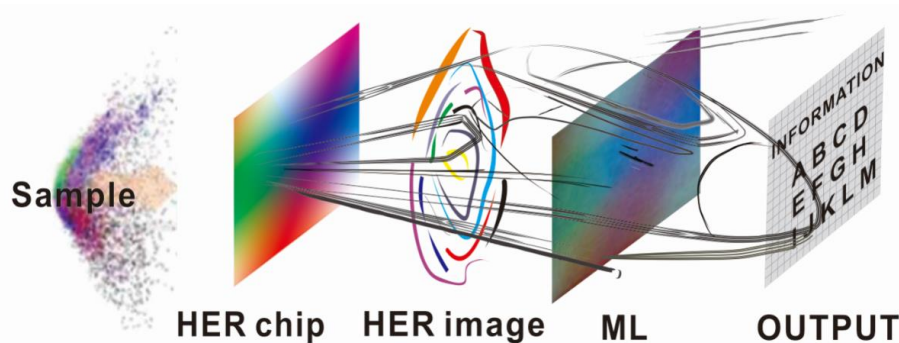
^b State Key Laboratory of Pollution Control and Resource Reuse, School of the Environment, Nanjing University, Nanjing 210046, China

^c Shaanxi SIER Biotechnology co. LTD, Dushizhimen D Building, Jinye Road, High-tech Zone, Xi'an, Shaanxi Province, 710077

^d Big Data and Urban Spatial Analytics Laboratory, Tongji University, Shanghai 200092, China

ABSTRACT: Machine learning (ML) has brought significant technological innovations in many fields, but it has not been widely embraced by most researchers of natural sciences to date. Traditional understanding and promotion of chemical analysis cannot meet the definition and requirement of big data for running of ML. Over the years, we focused on building a more versatile and low-cost approach to the acquisition of copious amounts of data containing in a chemical reaction. The generated data meet exclusively the thirst of ML when swimming in the vast space of chemical effect. As proof in this study, we carried out a case for acute toxicity test throughout the whole routine, from model building, chip preparation, data collection, and ML training. Such a strategy will probably play an important role in connecting ML with much research in natural science in the future.

Keyword: machine learning, toxicity test, high-throughput experimentation, inkjet printing, enzyme reaction chips



Abstract Graphic: A highway between toxicity perception and machine learning (ML). In a built highway, a sample was imaged by numerous enzyme reactions on a high-throughput chip (HER chip); and its information on acute toxicity was rapidly perceived on a trained CNN model. Here, the simple and effective HER chip just likes a high-speed rail for transportation of data between matter and ML.

31 Introduction

32 The relationships between things are the important objects of natural science research. Researchers have
33 created various research methods and means to reveal and quantify these relationships (1-3). After hundreds
34 of years of development, it seems that we have built a powerful knowledge system. While we also found that
35 most of the system is apt to describe the direct relations in some very simple phenomena. There is a primary
36 fact that most natural processes are controlled by the interactions of numerous factors. Some typical
37 examples are the reaction effects caused by the complex relationships, such as environment pollutions (4, 5),
38 health risk assessment (6), catalytic effects (7), toxicity (8), etc. Therefore, the exploration of these complex
39 relationships plays a decisive role in accurately grasping many natural laws in the future. It is also the
40 inevitable development direction of natural science. At present, there are not many strategies for scientists in
41 this direction, and particularly are those being adopted by ordinary researchers conveniently.

42 In recent years, machine learning (ML) has been developing rapidly. In many areas including business
43 and society management, the ML application has achieved a lot of meaningful innovation (9-11). This is due
44 mainly to some distinctive capabilities of ML, e.g., the outstanding performance on handling complex
45 systems that are hardly tamed on the base of existing knowledge (12-14). Most reaction effects are typically
46 complex processes, and we may use ML to explore the relationship between them.

47 In the course of understanding complex systems, the algorithm of ML, especially deep learning (DL),
48 mainly executes supervised training (15). The basic strategy is to collect and obtain a big database that
49 describes the research object, then to build a neural network consisting of numerous parameters
50 (generally $>10^7$), later to raise the model with training on the obtained data (15, 16). In this process, the
51 acquisition of a large amount of data is a key step. In today's torrent of artificial intelligence, there has been
52 a good breakthrough in the algorithms and hardware for this kind of research. However, most of traditional
53 experiment technologies are costly and low-efficient in the acquisition of required big data. Therefore, the
54 method of efficiently obtaining the data of the research objects will be very important to implement the ML
55 strategy. Even researchers need further to break through the understanding of the concept of scientific data.
56 And be aware that the data used for ML may be quite different from the traditional scientific data, although
57 those two kinds of data may all come from the same research object.

58 To obtain the data for the application of ML, there are some new technologies being improved or created
59 in the future work. High-throughput experimentation (HTE) seems to be one of the best ways to meet the
60 demand. The HTE, appearing in its powerful abilities in parallel operations and data production, is being
61 adopted by some researchers (17). But we also see that today's HTE technologies are developing towards
62 the expensive and the specialized, so that its recognition to most scientists is far less than that of the
63 traditional experimental technologies. Moreover, current HTE technologies are always pursuing the
64 miniaturization and parallelization of the routine experiments. It is very difficult to surpass the original
65 understanding of the research objects due to the same perspective. Hence when acting on the ML, most HTE
66 techniques just have to improve its tricks even principles.

67 One of smart HTE technologies is ink-jet printing technology (IJP) (18). The IJP usually uses the CMYK
68 model (referring to cyan, magenta, yellow and black) to combine different chemical factors by regulating the
69 accurate output of each ink (19). Viewing from a point of chemical operations, we can state that the essence
70 of the IJP is a super-efficient operation to fulfill the transport of reactants. Relying on the IJP, plenty of
71 parallel reactions will be established on a planar carrier by precise positioning of chemical or biological
72 substances, which will generate a large amount of reaction data in a moment (18, 19). Sophisticated IJP
73 experiments have great potential to meet the data needs.

74 Following the above exploration strategy, some specific cases will be implemented to evaluate its
75 performance. Considering experimental conditions and technical reserves of our laboratory in recent years,
76 we will try to explore the relationship between acute toxicity (Ac-tox) and enzyme reaction, and verify the
77 effectiveness of the ML approach.

78 The Ac-tox is an important factor in comprehensive evaluation in many areas including environment, food,
79 medicine, biology, etc. (8). Currently, general Ac-tox tests almost involve biological indicators, including
80 fish (20), mites (21), algae (22), microorganisms (23) or other biomarkers (24). The overall experiments
81 follow a route containing many tedious operations of continuous culture and analysis. When evaluating
82 some samples with complex composition, researchers often select some typical toxicants (e.g. mercuric
83 chloride, 3,5-Dichlorophenol, etc.) as reference substances to reflect the bio-toxicity indirectly (25). These

84 traditional methods usually involve excessive costs in terms of instruments and time, and also hinder the
85 presentation of Ac-tox test in many cases.

86 In the testing techniques of Ac-tox, LBAT test (luminescent bacteria acute toxicity test) is a smart and
87 typical one. This technique is highly sensitive to most toxicants in a short running time. And that, the
88 enzyme action and the chemical condition in the test are also similar to that in many higher mammals (4, 5).
89 In a LBAT test (25), a sample was mixed completely with the diluent of luminescent bacteria. The
90 intracellular luciferase (Luc) in bacteria was damaged by toxicants, and the bioluminescence was inhibited.
91 Afterwards, the Ac-tox was assessed by luminescent inhibition rate (LIR), referring to the
92 intensity variation in bioluminescence before and after being exposure to toxicants.

93 In the following work, we will try to build a simple and effective HTE bridge between Ac-tox test and ML.
94 The bridge, grasping the common properties of the data supplied from the HTE tests and that applied in the
95 ML algorithm, is capable of providing Ac-tox data to ML modelling quickly and massively. As emphasized,
96 the success of this work depends mainly on the following two points, how to operate a large quantity of
97 identifiable reactions, and how to build a proper ML model to apply these reacting data. Below, we will
98 elaborate more on the practices of our strategy.

100 Results

101 Overall scheme

102 In the experiment work of this paper, we focused on how to fast acquire the Ac-tox dataset, and also tried to
103 construct a suitable ML model to predict the Ac-tox. The particulars are as follows.

104 At first, following IJP technology, a kind of high-throughput enzyme reaction chip (HER chip, Fig. 1A)
105 was prepared on a modified inkjet printer (Fig. S1). On the prepared chip, there are numerous varied
106 micro-reaction dots containing accurate default of 6 enzymes or chemicals (listed in Table S1), including
107 lead acetate, sodium citrate, glucose, glucose oxidase (GOD), catalase (POD) and 2, 6-dichlorophenol
108 Indophenol sodium (DCIP, a blue-violet azo dye). On a reaction dot, these reagents join in a given enzymatic
109 process that mainly refers to a glucose-oxidized reaction. The pivotal conversion is the oxidation of glucose
110 to form oxygen radical [O] in catalyzing of GOD and POD, and the acceleration of [O] on the decoloration
111 of DCIP. In the process of the chip preparation, we used a designed template (500×500 dpi, Fig. S2A) to
112 conduct the printer to distribute accurately reactant liquids on a selected PVC-substrate. Following
113 air-drying in room conditions, we obtained some chips consisting of about 2.5×10^5 reacting dots.

114 When the chips were used for testing, the tested sample, as a solution, was uniformly dispersed onto the
115 chip; and then, the enzyme processes in each dot on the chip would be activated or inhibited in varying
116 degrees. The reaction results were visually exhibited by the discoloration of DCIP. Taken as a whole, a
117 richly-colored image (named HER image, Fig. 1A) emerged on the HER chip. Due to the massive amount of
118 the toxicological response results on the chip the HER images recorded the Ac-tox information of the tested
119 sample in an inapprehensible style.

120 For collecting a sufficient number of HER images for the later ML, we selected 4 typical toxicants as
121 original candidates for ink solutions (HgCl_2 , PbNO_3 , Tet and SM2-Na, Table S2). All thousands of
122 distinctive toxic samples were produced with mixing precisely the fours in IJP. This mixing process, also
123 including the enzyme reaction, actually takes place on the HER chip efficiently, and the results displayed on
124 the HER images.

125 What's more, we also directly collected Ac-tox data of all toxic samples via a modified LBAT test (Fig.
126 1B). The basic operation of this approach was to integrate the bacteria onto hardware platforms, which was
127 inspired by existing luminescent sensors (26). The Ac-tox reaction between the sample and luminescent
128 bacteria was realized by another IJP operation. Here, toxic samples as inks were printed regularly on several
129 nutrient plates for culturing luminescent bacteria uniformly. And the change of the luminescence intensity
130 (FI) on the plates was recorded by continuous photographing. In the end, the calculated LIRs (ranging from
131 0 to 1) as Ac-tox data were provided for the next ML section.

132 Eventually, a convolutional neural network model (15) (CNN, Fig. 1C) was adopted to perform regression
133 analysis between the achieved HER images and LIR data. The learnable parameters of the model were
134 iteratively adjusted by an error-backpropagation algorithm. The performance of the trained CNN was tested
135 by using new HER images (test set) as the input to the network. The predicted LIRs were compared with the

136 factual ones to estimate prediction accuracy.

137 138 **Producing HER images**

139 Preparing a greater quantity of HER chips is a foundation for building the ML dataset. We thoughtfully
140 designed a combined template composed of 20×20 HER chips (Fig. 2SB). Under the guidance of this
141 template, a batch of 400 HER chips was produced in an IJP cycle. After 4 cycles, 1600 HER chips (ie.,
142 4×400) were obtained.

143 On these chips, how to make them accurately and rapidly react with the test samples was also a technical
144 challenge. In such situations, the IJP, as an efficient means of distributing material, still was a good choice.
145 In details, we designed a sample template (Fig. 3A) that contained 400 individual recipe units (arranged as a
146 20×20 matrix) consisted of three C/M/Y layers. The intensity of these three colors was directly related to the
147 concentration of 'inks' in a unit. When loading several toxicant solutions in separated cartridges on a printer
148 (assembled rules see in Table S3), it is accessible to create larger numbers of different test toxicants (ratios
149 listed in Table S9) on all specified units with the guidance of the template software. When these units are
150 precisely set to 1600 chips (Fig. S3B), we got the same number of HER images (Fig. S4 and Table S5)
151 followed performing a large batch of reactions and scanning them.

152 The richness and diversity of the information on HER chip are worth investigating. In Fig. 2A, the pattern
153 on a HER chip changed before and after reacting, which was attributed mainly to all the differences of
154 abundant reaction dots on the chip. As to the reaction course on dots (Fig. 2B), the GOD and POD were
155 inactivated by Pb^{2+} and Hg^{2+} , and then the fading process of the dye (DCIP) was inhibited. This process may
156 be tuned by pre-existing substances on HER chips (such as Na-Citrate, Tet, SM2-Na), or others in the
157 samples. Then bring out a result of the diverse enzyme reactions.

158 The information in HER images involves at least three aspects. The first is the distribution of pattern and
159 color, which is unique for a given test sample. The second is derived from the specific chemicals at any dots
160 of a HER chip. When we got a HER image, the specific chemical conditions will clarify quite a few temper
161 of the enzymatic reaction. The third kind of information grows out of the cluster of numerous HER images,
162 which is capable of connecting magically many seemingly-unrelated factors. When an image was digital
163 (Fig.3C), these kinds of information are exhibited as 3 color dimensions (RGB, Red, Green, Blue) of pixels.
164 And each dimension is quantified in a range of 0 to 255 (0 corresponds to black, 255 to white). These RGB
165 values indirectly reflected the toxicity characteristics of test samples, which are the data basis for the later
166 ML modelling.

167 168 **Collection of LIR data**

169 Although the LBAT test usually more available than others, it is still a time-consumed and costly operation,
170 especially for testing thousands of samples. Thus, rapidly getting the Ac-tox data is important for us to
171 enhance the efficiency of data acquisition.

172 In this case, we once again introduced the IJP tool into the improvement of the LBAT test. For some steps,
173 we took advantage of its ability to transfer matter efficiently. In practice, before toxic reacting, the
174 luminescent bacteria was prepared into a bio-ink and evenly printed on 4 plates (Fig. S5A). The medium
175 was covered with bacteria uniformly released blue-green light at 450-490 nm in the dark, forming
176 bioluminescence substrates. After the toxics directly act on the substrate, the luminescence process might be
177 inhibited, and the FI variation was visually recorded on the plates. Here, by adopting the same toxic
178 combination with Table S3, the given 1600 samples were printed on 4 bio-substrates following the layout of
179 another template (Fig. S3A). To accurately record the fluorescence changes on whole substrates, they were
180 immediately placed in a light-proof incubator for taking continuous pictures (Fig. S5B). Ultimately, the
181 Ac-tox of all samples would be evaluated by the brightness variation of the collected luminescent photos
182 (Fig. 3).

183 For toxicity assessment, we refer to an existed standard of luminescent bacteria tests (25). By
184 analogy with the calculation in the standard, the LIR was calculated by the variance rate of the gray level at
185 each reacting cells throughout the photos. Besides, for optimizing an appropriate reaction time for the
186 Ac-tox evaluation, an experiment referring only to the 4 toxicants ($HgCl_2$, $PbNO_3$, Tet or SM2-Na) was
187 carried out. And detailly, they were in sequence printed and cultured according to own templates (Fig. S6),
188 and implemented a full coverage from 0 to 100% of concentration. By observing the gray evolution of these

4 strips, we found their gray no more changed within 5 to 30 min. This indicated that the Ac-tox actions of the toxicants on the luminescent bacteria completed within 5 min. Here, we chose the photos of the reaction time of 5, 15 and 30 min to calculate the data of the LIR (see Method section for calculation details), and listed them in Table S9.

Prediction of Ac-tox in CNN

A CNN model based on regression calculations (see in Table S7) was used to predict the Ac-tox. Selecting CNN as a ML model is compatible with the obtained data in image style. We found that CNN is good at extracting local features of images, and capturing the difference of these features in RGB values sensitively (10). Correspondingly, CNN possesses the potential for exploring the non-linear relation between LIR and HER images. In the CNN structure used in this study, the key functional blocks of machine learning are convolution layers and below nonlinear activation function.

$$\begin{cases} y_i = \sum_j w_{ij} x_j + b_i \\ y'_i = \max(y_i, 0) \end{cases} \quad (1)$$

Where x and y are input and output vectors, respectively; and w and b are synaptic weights and biases, respectively (11). Where y'_i is an activation function (ReLU) for neurons in the hidden layer of the network. The ReLU could avoid “gradient disappearing” during the computing processes (27). The principle of training a traditional network is to continuously optimize the network in w (and b) (11); this means a lot of training time in learning parameters. However, CNN can reduce the parameters in the training process through sharing weight and shrinking convolution kernels(15). The error-back-propagation algorithm can match the prediction value and factual value to the closest degree(11, 28). And the trained framework is capable to avoid over-fitting problem by introducing dropout layers (reducing the dimension via eliminating the relevant parameters) and regularization layers (10, 28).

At training stage of the CNN, the previously-acquired HER images and LIR data were served as a dataset. All the HRE images (GRB format) were adjusted to a size of 100×100 dpi and uniformly deducted background values. In Fig.4, when a HER image is taken as the input, the network first processes the images through multi-rounds of convolution, ReLU nonlinearity, and max pooling layers. And then the predicted LIR value (regularized to 0 to 1) is output through a fully-connected layer.

The predictive accuracy for LIR was evaluated using root mean squared error (RMSE) and the coefficient of determination (R^2) of test set via linear regression. As shown in Fig. 5A, the RMSE is 7.5% and the R^2 value is 0.9203 without overfitting, which means we obtained a satisfying result on the regression of the HER images and the LIRs. A confusion matrix for classification (5 levels, Fig. 5B) is drawn based on the prediction results of the test set. Each element (i, j) of the matrix represents the probability of predicting class j given that the true Ac-tox class i (Table S9). The accuracy rate for the classes of median-toxic, severe-toxic, and highly-toxic reached 87.6, 73.7, and 93.9%, respectively; but only 4.5 and 56.5% of the predictive accuracy rate for the classes of non-toxic and low-toxicity. This may be due to the small number of the training data in these two levels limiting the performance of the CNN. Additionally, we randomly selected 50 new samples to verify the prediction accuracy on a small set (Fig.6). It can be found that only 6 out of 50 samples were predicted to outliers (prediction levels deviate from the real ones), and that the biases are only one level.

Discussion

The execution of our experiments benefited from the introduction of the IJP technology to prepare the high-density HER chips. Millions of independent micro-reactions were constructed easily by using a precise combination of reagents on a two-dimensional plane. Over the years, we have been bending ourselves to explore this technology, named chemical neural network chip (ChNN) in our lab habitually. On the other hand, in the field of analytical chemistry, the synthesis of numerous color (or fluorescence) indicators have accumulated lots of knowledge and products. They are contributing a treasure trove of creating many novel HTE detectors. Therefore, IJP and indicators inspire us to stare other biochemical effects. For example, Brady's team reported in Nature (Sep., 2017) that certain compounds produced by the intestinal flora had

potential physiologic role in humans (29). Following our experimentation to combine 10^8 magnitude of nutrient conditions, a proper HTE chip for surveying intestinal floras will promptly expand the searching space and simplify the experimental means. In addition, there are many important reaction processes in the field of environment or medicine. We can also build large-scale combinatorial systems for exploring huge space of more reactant types and conditions. This maybe accelerates us make new interpretations for the biological and chemical reaction relying on a large effect database.

At the same time, we are also thinking: what is the implicit link between HER images and the toxicological effects? This link may be derived from their commonality in the inhibition of the enzyme. The commonality is usually so complex that, to date researchers hardly find specific mechanisms to accurately describe it. However, we find increasingly that a neural network with millions of nodes may be a good describer of a complex effect. In other words, we can digitally describe a complex chemical process using a network with sufficient depth and breadth. Whereas, to successfully train this huge network, a satisfactory data set is necessary. Here, researchers can refer to the data amount of this work, about 1.6×10^{11} points, (ie., 10^8 points \times 1600 chips). Practically, the tech-nodus for introducing ML in some natural science often lies in how to gather sufficient datasets.

Here, we selected only 4 typical toxicants and their mixtures to build an Ac-tox database. Choosing such a small-scale dataset is more conform to the focus of current work, verifying the feasibility of the proposed strategy and experimentation. And while conducting constructions of many new devices and algorithms, a reasonable exploration in a small and complete data space will be affordable for us in terms of time cost. Obviously, the experimental operation of this study did not limit the variety of substances to be explored. It is foreseeable that mixtures with more-complicated components will also follow this pathway smoothly. For instance, beverages, drugs, urine, and they are the ordinaries in natural science.

What is worth mentioning, the obtained HER images pose formatted patterns following the precise control of the conditions at each dot on the chip. This is obviously different from usual image datasets supplying ML, such as these pictures of cancer pathology, fundus scans, or street view. These databases often contain at least thousands to millions of pictures, which are much larger than the training set in our job. But it needs to be pointed out that the amount of effective information in these images is too low. One vivid description is that the ordinary images are similar to some stone bombs collected from various places, but well-conceived images are modern standard ammunitions. For the “ML cannon”, their efficiency will be very different.

In this study, lots of bio-effect data were easily produced by HER chips. But we can say humorously that these data are “useless”. That is, we hardly extract directly the toxicological info from the HER images only with the existing knowledge system. Nevertheless, it is because we do not pursue “common-sense understanding and application” of data that allows us to focus more on creating cost-effective and efficient ways of data acquisition. This starting point may also be an appropriate strategy for machine learning to explore various scientific issues in the future. Because there are still too few databases that are directly understood by human and meet the appetite of ML.

Briefly, we have initially attempted to establish machine learning approaches of exploring the relationships among complex reaction processes. And adopting a smart experimentation of luminescent bacteria, we demonstrated the validity and efficiency of CNN modelling. The key to this approach is creating powerful means to actively produce mass of new data to describe the research objects. Also, the introduction of ML may provide other researchers a new thought for the study of other complex reaction effects.

Materials and Methods

All of the chemical reagents listed in Table S1-2 were (analytical grade, $\geq 99\%$) purchased from Aladdin Sigma-Aldrich. *Photobacterium phosphoreum* (T3 spp.) was purchased from Nanjing Institute of Soil Science. A white PVC plate (A4, Guangzhou Chongze Tech. Co.) was used as the printing substrate. A commercial ink-jet printer (R230 printer, Epson Company) was reformed. An image scanner (S48) was purchased from Plustek Technology Co., Ltd., China. A high-sensitivity CCD camera (A75, Canon Company) that can be controlled by a computer was used to record FI variations of luminescent bacteria.

Reform of ink-jet printer

291 A commercial ink-jet printer was reformed. It has the advantages of high accuracy, multiple channels,
292 non-contact, and no heating (ensuring bio-ink activity). As shown in Fig. S1, the paper entry mechanism of
293 the printer was modified as a fixed-platform **1** and it has a positioning slot **3** that can fix the substrates. Then,
294 the printer's driveline was modified. That is, the printing head **6** is reciprocated along a horizontal guide rail
295 **5** under the control of an additional stepping motor **7**, while it can also advance along a vertical guide rail **4**
296 at a constant speed. Additionally, the printing head has six cartridges refer to color channels of C/M/Y. When
297 working, the cartridges are emptied to be applied to fill solutions containing enzymes or chemicals (Table S
298 1 to 2).

300 **Producing HER images**

301 **Preparation of printing solutions**

302 For preparing the HER chip, 6 solutions containing enzymes or chemicals were adopted, including
303 $(\text{CH}_3\text{COO})_2\text{Pb}$, sodium citrate, POD (≥ 300 units/mg), GOx (≥ 100 units/mg), Glucose and DCIP (see in
304 Table S1). A series of precursor solutions were prepared in given concentrations respectively. Particularly,
305 the surface tension of the inks is adjusted to ensure the normal operation of the printer. Here, ethylene glycol
306 monobutyl (DGBE) was added to lead acetate, sodium citrate, glucose, and DCIP, respectively. For the
307 preparation of GOD or POD ink, PEG-20000 and *tert*-butanol were added to the enzyme solution (1 mg/mL
308 of protein) in phosphate buffer (pH 7.5, 50 mM) (19). All inks were adjusted to exactly match the original
309 ink ($\sim 45 \text{ dyn mL}^{-1}$).

310 **Design of HER-Chip template**

311 In Fig. S2A, single HER-chip template is designed as a rectangle (500×500 dpi) composed of 6 color layers,
312 in which CMY refers to three inks: regular cyan, magenta, and yellow. According to the color distribution
313 (pre-set CMY values), layers **1-3** indicates that the output of each ink ranged 0-100% in steps of 1%, while
314 the inks on layers **4-6** are in a constant output of 100%. All the layers were corresponded to the enzymes (or
315 chemicals) as listed in Table S1. At last, this CMY model will generate a color space theoretically containing
316 2.5×10^5 dots by various combinations of these layers. Besides, a composition template containing 400 HER
317 chips also was designed in Fig. S2B. The chips are spatially arranged in a 20×20 matrix, and each one is
318 made up layers **1-6**. By printing 4 pages (one page 400 chips), 1600 HER chips were parallelly prepared.

319 **Design of sample template**

320 A sample template (Fig. S3a) contained 20×20 individual recipe units was designed, and each unit
321 (10.0×10.0 mm) represents a mixed sample of 3 toxic compounds (selected from Table S2). All CMY layers
322 in the template respectively contain a subtle linear-gradient of color (ranged from 0-100%) in different
323 directions. By arranging multiple inks in the template (assembled rules see Table S3), 1600 mixed-samples
324 were formed and printed.

325 **Preparation of HER chip**

326 In a typical step, the cartridges were washed with distilled water and ethanol, and 6 inks (listed in Table S1)
327 were added to the cartridges. The selected PVC substrate was placed smoothly on **1**, and fixed at a
328 designated location. During printing, the nozzles were guided by the composition template (Fig. S2B) to
329 print the inks on the substrate. Specially, by stacking the layers, 6 inks in Table S1 were combined along
330 certain distribution directions and quantities. For in-situ mixing of the reactants on the HER chip, the
331 obtained HER chips were sprayed with pure water in an ultrasonic actuator (droplets with size of about 3 to
332 $5 \mu\text{m}$) followed by air-drying. Then, all the resulting chips were placed in an airtight vessel with deoxidant in
333 the dark.

334 **AC-tox reaction between HER chip and samples**

335 All the Ac-tox reactions between the HER chip and sample were carried out by positioning overprinting
336 (shown in Fig. S3B). Before reacting, 4 toxic compounds (HgCl_2 , PbNO_3 , Tet and SM2-Na, listed in Table
337 S2) were prepared into a series of solutions (in 2% NaCl), and added to the cartridges as original inks.
338 Meanwhile, one of the prepared substrate comprised of 400 HER chips was placed and fixed on **1**. During
339 printing, the 4 toxicant solutions as ink were distributed accurately following the guidance of the template in
340 Fig. S3A. Wait for the chip to dry (wait about 30 seconds), the 1600 HER images (see in Fig. S4) are
341 accurately scanned by a commercial laser scanner.

342 **Collection of AC-tox data**

Preparation of nutrient plates

A classically formulated Sea Water Broth (SWB) culture medium was prepared as the nutrient plate. SWB contained: yeast extract, 2.5g; tryptone, 2.5g; Na₂HPO₄ ·12H₂O, 6.3 g; KH₂PO₄, 0.5g; NaCl, 15 g; agar, 10g and pH 6.8-7.2 in 400mL distilled water. The obtained mixed suspension was sterilized in a sterilizer at 394 K for 20 minutes, and then was evenly distributed to four rectangular glass dishes (10×10 cm), cooling to room temperature. Then, these obtained nutrient plates were preserved in a sterilizer box for later use.

Preparation of luminescent bacteria diluent

Freshly prepared *Photobacterium phosphoreum* (T3 spp.) was quantitatively inoculated into a SWB medium (200 mL, without agar), and then it oscillated for 14 h at 293 K in a constant temperature shaker for further replication. Then, the reconstituted bacterial suspension (1.0×10⁸ cells mL⁻¹ luminous bacteria) was diluted (10:1) as a bio-ink for the latter LBAT test.

Modified LBAT test

In preparation, four prepared 10×10 cm nutrient plates were placed on the designated areas of a sterile glass plate, and 5 mL of bio-ink was added to the cartridge. Then, the bio-ink was uniformly printed on the plates forming bio-substrates, and wait for 4 hours to make the bacteria to light steadily.

Next, the toxicity test still was applied on above substrates (see in Fig. S5). Four sample templates are arranged parallelly on these substrates, each substrate corresponds to 20×20 samples. According to the assembled rules in Table S3, aforementioned HgCl₂ etc. toxic solutions (Table S2) as original inks once again were respectively printed on the substrates, appearing 1600 reacting cells. Then, a high-sensitivity CCD camera was used for continuous photographing (One shot every 1 minute, continuous shooting 12 hours) and a series of bio-luminescence photos (Fig. 3) were acquired. Shooting parameters see in Table S6. In addition, a blank control experiment on regions without printing toxicants was conducted simultaneously.

LIR Calculation

Average gray values of all the reacting cells on pictures in Fig. 3 were extracted using *Matlab*. Variance rate of gray level on the same cell at various times (t = 0, 5, 15, 30 min) was used to represent the LIR of the sample. The calculation process as follows:

Calculate the luminous intensity correction factor (f_{kt}-value) from the measured gray value using Equation (1). This factor is used to correct the initial values I₀ of all the samples before they are used as reference values. It can be used to correct the luminescence intensity change of CK regions (only luminescent bacteria without printing the samples) due to the evaporation of water from the medium.

$$f_{kt} = \frac{G_{kt}}{G_0} \quad (1)$$

Where f_{kt} is the luminous intensity correction factor, G_{kt} is the average gray value of CK regions at t = 5, 15 or 30 min, G₀ is the average gray value of the CK region at t = 0 min.

$$G_{ct} = f_{kt} \times G_0 \quad (2)$$

Where G_{ct} is the corrected value of G₀ before the addition of the test sample.

The LIR using Equation (3):

$$\text{LIR}\% = \frac{G_{ct} - G_t}{G_{ct}} \times 100\% \quad (3)$$

G_t is the average gray value at t = 5, 15 or 30 min after the Ac-tox reaction. LIR is luminescent inhibition rate of one of the samples. Here, at different shooting time pictures, the average gray values of the same samples were extracted from the same reacting cells. Similarly, LIRs of other samples were calculated by the same way. And finally only the data of t = 15 min were used as the label for HER images.

Supplementary Materials

Fig. S1. The reformed ink-jet printer.

Fig. S2. Design of printing templates.

Fig. S3. Design of sample template; and application of the Ac-tox reactions.

Fig. S4. Obtained 1600 HER images.

Fig. S5. Collection of LIR data.

Fig. S6. Gray variations on the luminescence images.

Table S1. Configuration of inks on a single HER template Table S2 Shooting parameters.

Table S2. List of 4 toxic compounds.

Table S3. Assembled rules of 4 toxic compounds on the sample template.

Table S4. Physical properties of candidate print substrates.

Table S5. Coding numbers of 1600 HER chips (or images).

Table S6. Shooting parameters.

Table S7. Detailed architecture of CNN.

Table S8. Ac-tox evaluation standard.

Table S9. LIR data and sample composition.

Table S10. LIR data for training set (80%).

Table S11. LIR data for test set (20%)

Acknowledgments: Thanks to Chaoqun Zheng and Baoxin Zhai for their work in preparing the materials in the early stage. Especially, Qiannan Duan wants to thank her parents (Mr. Duan and Mrs. Wu), for their love, patience and selfless support over the years. Finally, we salute to the great physicist, Stephen William Hawking.

Funding: This work is supported by the National Natural Science Foundation of China (No.50309011) and the Scientific Research Foundation for the Returned Overseas Chinese Scholars (08501041585).

Competing interests: The authors declare no competing interests.

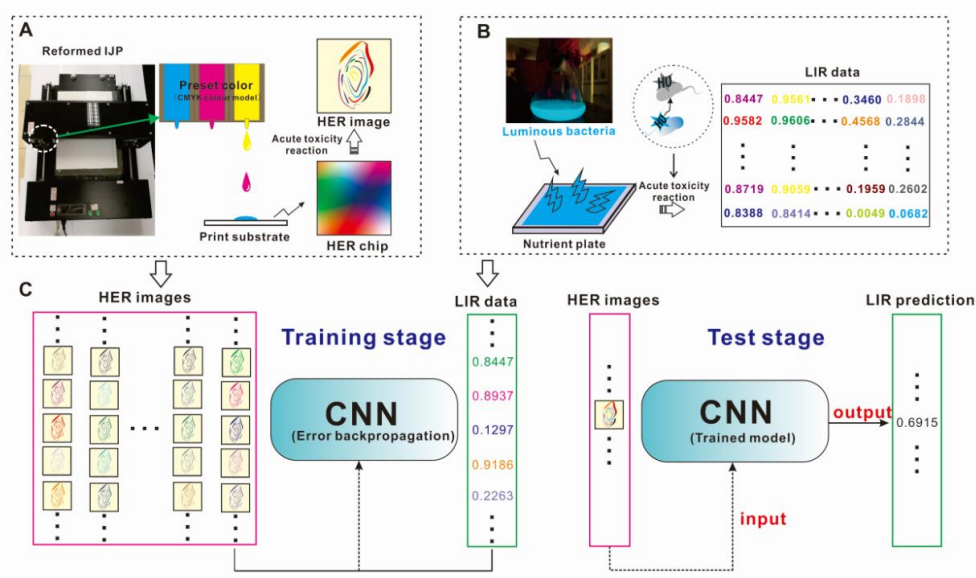
Data and materials availability: Additional figures, tables, and descriptions. Besides, the original HER images used for training and testing the models can be downloaded from an URL, <http://yunpan.snnu.edu.cn:80/#/link/3F8867BF29D30048668646809875892D>, with a fetch code: 6Wax. All the data that support the results of this study are available from the corresponding author.

References

1. S. Allesina, J. Grilli, G. Barabas, S. Tang, J. Aljadeff, A. Maritan, Predicting the stability of large structured food webs. *Nat. Commun.* **6**, 7842 (2015).
2. Y.-Y. Liu, Theoretical progress and practical challenges in controlling complex networks. *Natl. Sci. Rev.* **1**, 341-343 (2014).
3. J. Ruths, D. Ruths, Control profiles of complex networks. *Science* **343**, 1373-1376 (2014).
4. T. Wang, Y. Liu, D. Wang, Z. Lin, Q. An, C. Yin, Y. Liu, The joint effects of sulfonamides and quorum sensing inhibitors on *Vibrio fischeri*: Differences between the acute and chronic mixed toxicity mechanisms. *J. Hazard. Mater.* **310**, 56-57 (2016).
5. H. Hu, C. Jiang, H. Ma, L. Ding, J. Geng, K. Xu, H. Huang, H. Ren, Removal characteristics of DON in pharmaceutical wastewater and its influence on the N-nitrosodimethylamine formation potential and acute toxicity of DOM. *Water Res.* **109**, 114-121 (2017).
6. H. Wang, N. Wang, J. Qian, L. Hu, P. Huang, M. Su, X. Yu, C. Fu, J. Feng, Q. Zhao, Urinary antibiotics of pregnant women in Eastern China and cumulative health risk assessment. *Environ. Sci. Technol* **51**, 3518-3525 (2017).
7. L. Ward, A. Agrawal, A. Choudhary, C. Wolverton, A general-purpose machine learning framework

- 434 for predicting properties of inorganic materials. *npj Comp. Mater.* **2**, 16028 (2016).
- 435 8. D. Wang, Y. Gu, M. Zheng, W. Zhang, Z. Lin, Y. Liu, A Mechanism-based QSTR Model for Acute to
436 Chronic Toxicity Extrapolation: A Case Study of Antibiotics on Luminous Bacteria. *Sci. Rep.* **7**, 6022
437 (2017).
- 438 9. D. Ahneman, Predicting reaction performance in CN cross-coupling using machine learning (vol 360,
439 pg eaat7648, 2018). *Science* **360**, 613-613 (2018).
- 440 10. A. Esteva, B. Kuprel, R. A. Novoa, J. Ko, S. M. Swetter, H. M. Blau, S. Thrun, Dermatologist-level
441 classification of skin cancer with deep neural networks. *Nature* **542**, 115-118 (2017).
- 442 11. Y. Jo, S. Park, J. Jung, J. Yoon, H. Joo, M.-h. Kim, S.-J. Kang, M. C. Choi, S. Y. Lee, Y. Park,
443 Holographic deep learning for rapid optical screening of anthrax spores. *Sci. adv.* **3**, e1700606
444 (2017).
- 445 12. R. Gómez-Bombarelli, J. N. Wei, D. Duvenaud, J. M. Hernández-Lobato, B. Sánchez-Lengeling, D.
446 Sheberla, J. Aguilera-Iparraguirre, T. D. Hirzel, R. P. Adams, A. Aspuru-Guzik, Automatic chemical
447 design using a data-driven continuous representation of molecules. *ACS Cen. Sci.* **4**, 268-276 (2018).
- 448 13. Y. D. Hezaveh, L. P. Levasseur, P. J. Marshall, Fast automated analysis of strong gravitational lenses
449 with convolutional neural networks. *Nature* **548**, 555-557 (2017).
- 450 14. Y.-Y. Liu, J.-J. Slotine, A.-L. Barabási, Observability of complex systems. *P. Natl. Acad. Sci. USA.*
451 **110**, 2460-2465 (2013).
- 452 15. Y. LeCun, Y. Bengio, G. Hinton, Deep learning. *nature* **521**, 436-444 (2015).
- 453 16. I. Goodfellow, Y. Bengio, A. Courville, Y. Bengio, *Deep learning*. (MIT press, Cambridge, 2016),
454 vol. 1.
- 455 17. K. Troshin, J. F. Hartwig, Snap deconvolution: An informatics approach to high-throughput
456 discovery of catalytic reactions. *Science* **357**, 175-181 (2017).
- 457 18. L. Wang, J. Lee, M. Zhang, Q. Duan, J. Zhang, H. Qi, Fluorescence imaging technology (FI) for
458 high-throughput screening of selenide-modified nano-TiO₂ catalysts. *Chem. Commun.* **52**, 2944-2947
459 (2016).
- 460 19. Y. Zhang, F. Lyu, J. Ge, Z. Liu, Ink-jet printing an optimal multi-enzyme system. *Chem. Commun.* **50**,
461 12919-12922 (2014).
- 462 20. N. Klüver, M. König, J. Ortmann, R. Massei, A. Paschke, R. Kühne, S. Scholz, Fish embryo toxicity
463 test: Identification of compounds with weak toxicity and analysis of behavioral effects to improve
464 prediction of acute toxicity for neurotoxic compounds. *Environ. Sci. Technol.* **49**, 7002-7011 (2015).
- 465 21. M. Neves *et al.*, Biochemical and populational responses of an aquatic bioindicator species, *Daphnia*
466 *longispina*, to a commercial formulation of a herbicide (Primextra® Gold TZ) and its active
467 ingredient (S-metolachlor). *Ecol. Indic.* **53**, 220-230 (2015).
- 468 22. J. Villain, L. Minguez, M.-P. Halm-Lemeille, G. Durrieu, R. Bureau, Acute toxicities of
469 pharmaceuticals toward green algae. mode of action, biopharmaceutical drug disposition
470 classification system and quantile regression models. *Ecotoxicol. Environ. Saf.* **124**, 337-343 (2016).
- 471 23. S. C. Edberg, E. W. Rice, R. J. Karlin, M. J. Allen, *Escherichia coli*: the best biological drinking
472 water indicator for public health protection. *J. Appl. Microbiol.* **88**, 106S-116S (2000).
- 473 24. A. S. Thakor, R. Luong, R. Paulmurugan, F. I. Lin, P. Kempen, C. Zavaleta, P. Chu, T. F. Massoud, R.
474 Sinclair, S. S. Gambhir, The fate and toxicity of Raman-active silica-gold nanoparticles in mice. *Sci.*
475 *Transl. Med.* **3**, 79ra33 (2011).
- 476 25. D. ISO, 11348-3 (2007) Water quality—determination of the inhibitory effect of water samples on
477 the light emission of *Vibrio fischeri* (Luminescent bacteria test)-part 3: method using freeze-dried
478 bacteria. *PN-EN ISO.11348* (2007)
- 479 26. M. Mohseni, J. Abbaszadeh, S. S. Maghool, M. J. Chaichi, Heavy metals detection using biosensor
480 cells of a novel marine luminescent bacterium *Vibrio sp.* MM1 isolated from the Caspian Sea.

- 481 *Ecotoxicol. Environ. Saf.* **148**, 555-560 (2017).
- 482 27. C. Szegedy, W. Liu, Y. Jia, P. Sermanet, S. Reed, D. Anguelov, D. Erhan, V. Vanhoucke and A.
483 Rabinovich, Going deeper with convolutions, in *proceedings of the IEEE conference on computer*
484 *vision and pattern recognition* (IEEE, 2015), pp. 1-9.
- 485 28. D. T. Ahneman, J. G. Estrada, S. Lin, S. D. Dreher, A. G. Doyle, Predicting reaction performance in
486 C-N cross-coupling using machine learning. *Science* **360**, 186-190 (2018).
- 487 29. L. J. Cohen, D. Esterhazy, S. H. Kim, C. Lemetre, R. R. Aguilar, E. A. Gordon, A. J. Pickard, J. R.
488 Cross, A. B. Emiliano, S. M. Han, Commensal bacteria produce GPCR ligands that mimic human
489 signaling molecules. *Nature* **549**, 48-53 (2017).
- 490
- 491



493

494 **Fig. 1** Scheme for constructing a strategy between Ac-tox prediction and ML. (A) Preparation of the HER
 495 chip by IJP; and the HER image was received after the chip reacting with the test sample. (B) A modified
 496 LBAT test for collecting LIR data. (C) CNN for LIR prediction. At the training stage, the HER images and
 497 LIR data were as the training set. At the testing stage, some HER images of unknown samples as input, and
 498 their LIRs were predicted by the trained CNN.

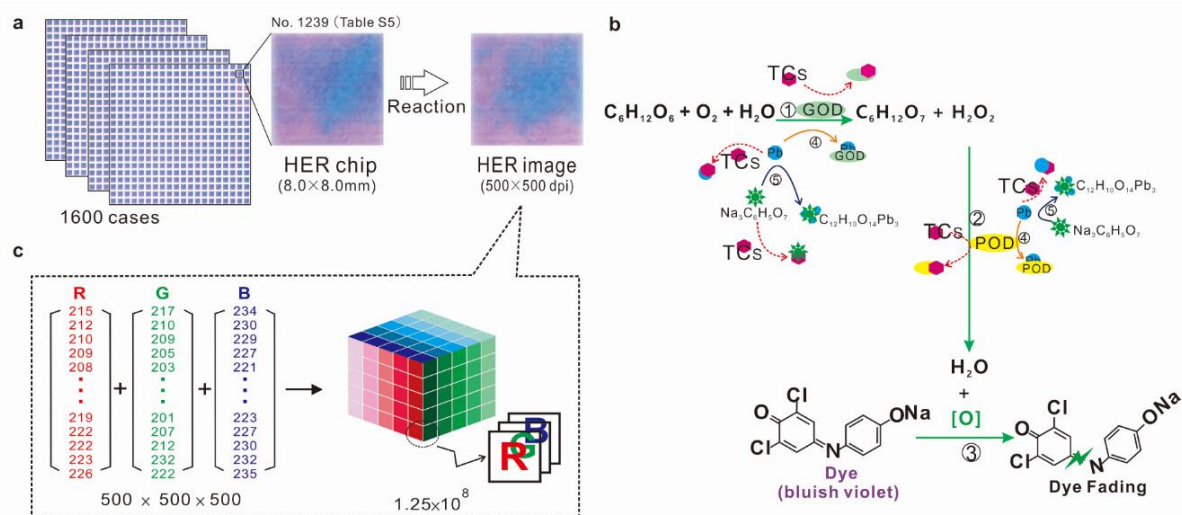
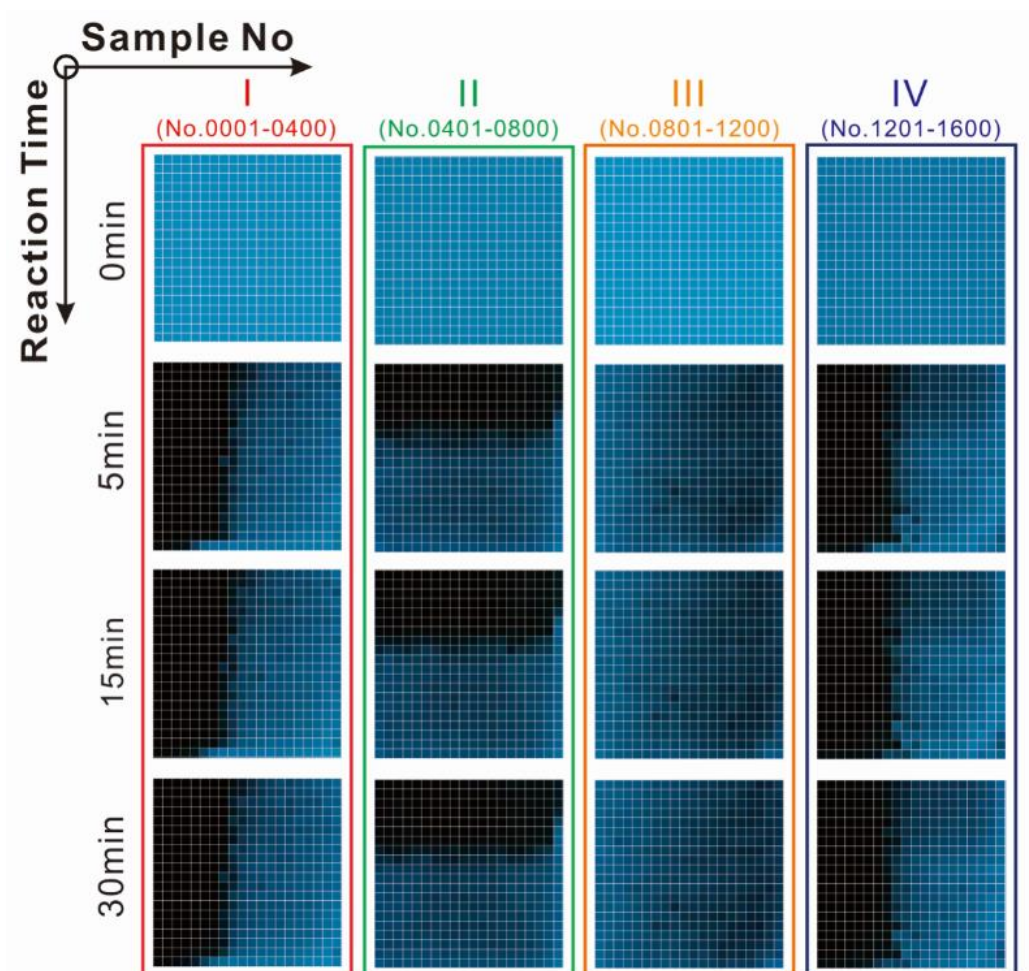


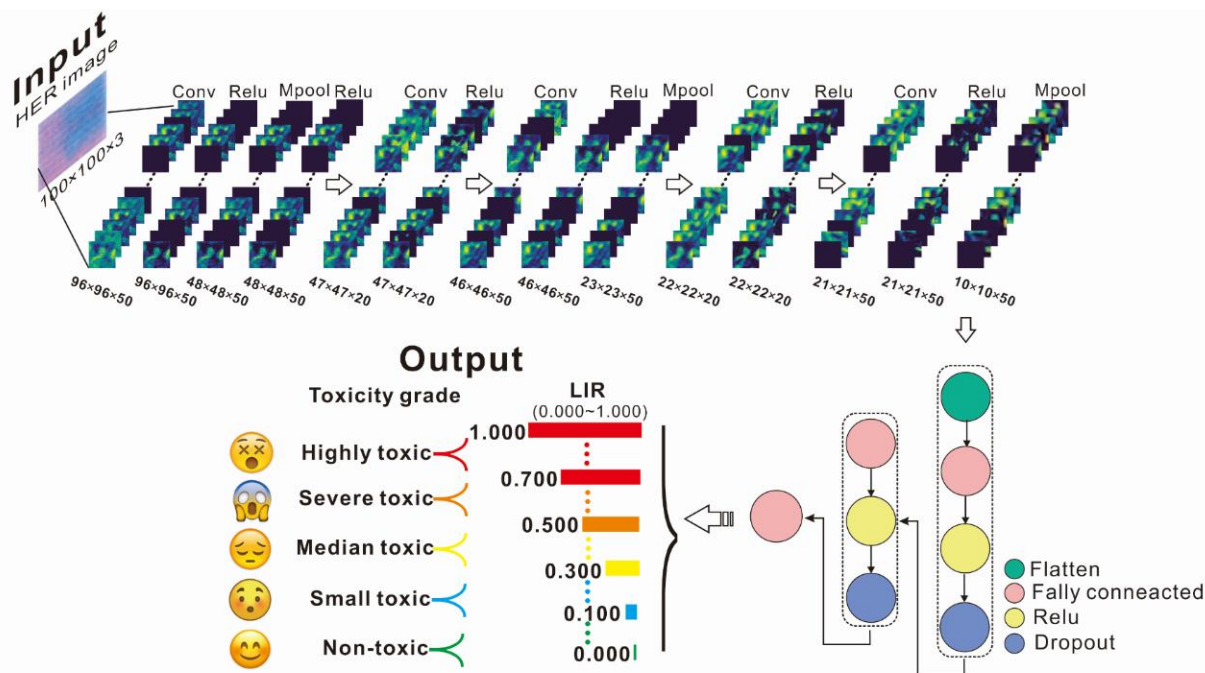
Fig. 2 (A) Obtained 1600 HER chips and appearance of a HER chip/image. (B) The enzymatic process in a dot on chip. Process 1 to 3: GOD catalyzes the oxidation of b-D-glucose into D-glucono-1, 5 lactone, and generates an equivalent amount of H_2O_2 . Then, DCIP is catalyzed by POD in the presence of H_2O_2 , exhibiting a dye-fading process (due to the C-N double bond in the structure of DCIP is broken by [O]). In process 4, GOD and POD are inactivated partly by Pb^{2+} , which inhibits the process 1-3. While Pb^{2+} combined with the citrates, the Pb^{2+} transforms into $C_{12}H_{10}O_{14}Pb_3$, and then, oppositely, 1-3 will be protected. In the meantime, the toxic compounds (TCs) in the sample maybe participate in all the process 1-5 (red dotted line), activating or inhibiting the 1-3. (C) Color dimensions of the HER image. In our experiment, the number can reach about 10^8 .

500
501
502
503
504
505
506
507
508
509
510



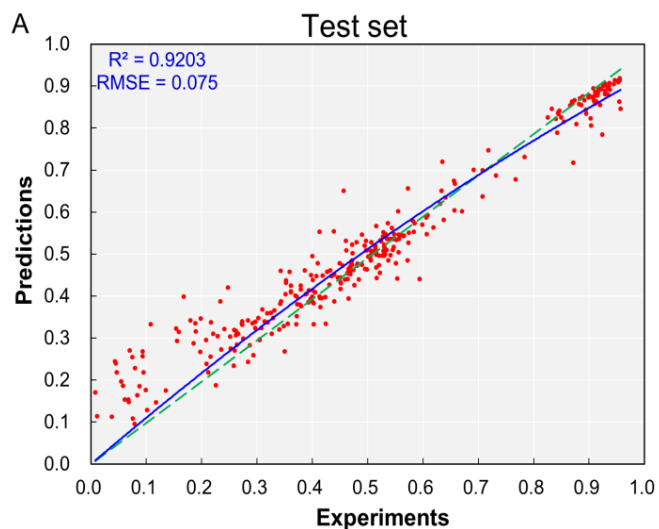
512
513
514
515

Fig. 3. Bio-luminescence photos at $t = 0, 5, 15$ and 30min , respectively. The photographing parameters are listed in Table S6.



516
517
518
519
520
521
522

Fig. 4. CNN framework for Ac-tox prediction based on HER images. The network is a regression-based CNN architecture. Data flow is from left to right: a HER image (No.0001 as a case) is taken as the input, the network first processes the image through five rounds of hidden layer, including convolution, ReLU nonlinearity, and max pooling layers. Then, the data flow through two fully-connected, ReLU and dropout-regularization layers. The output layer will give out the predicted LIR. Meanwhile, 5 toxicity grades also are as output in this CNN framework.



523

524

525

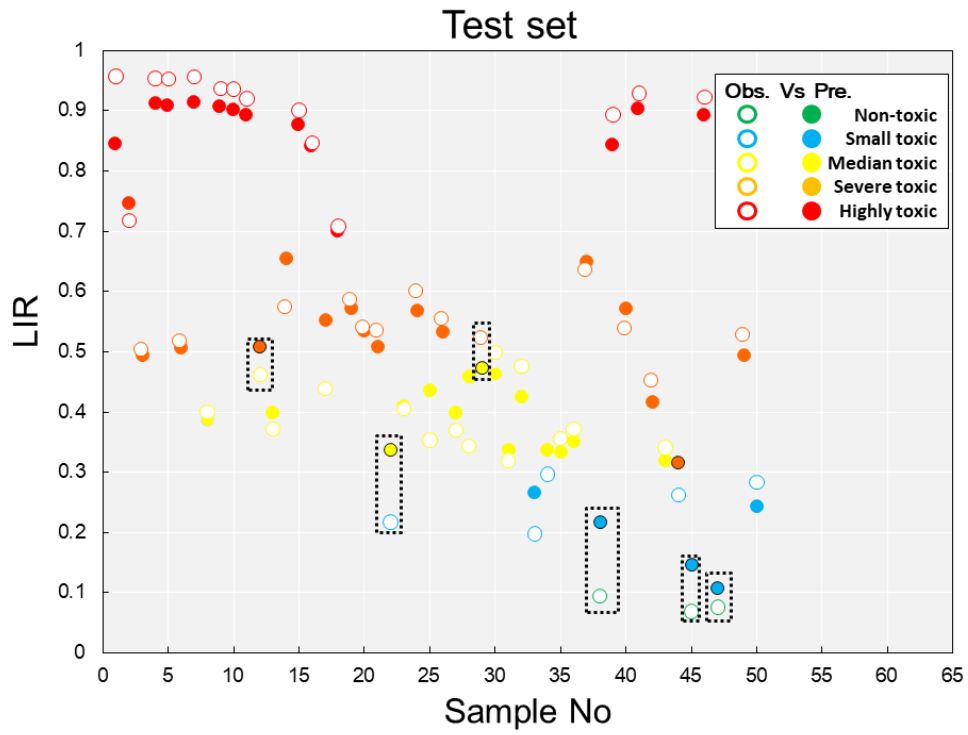
526

527

528

529

Fig. 5 Performance of the CNN framework. (A) Test set performance plots. Observed vs. predicted plots of LIR were predicted by the CNN. For the model, an 80/20 split of training and test data (Table S10-S11); and only the test set shown in plots. Superiority of the algorithm was evaluated by linear regression analysis: RMSE, root mean square error; R^2 , coefficient of determination; dashed line, $y = x$ line; solid line, Loess best-fit curves. (B) Confusion matrix illustrating the performance of the CNN.



530
531
532
533
534

Fig. 6 An Ac-tox level prediction for 50 random samples. Solid or open dot is the predicted or observed LIR data, respectively. Predicted outliers are circled in dotted line.